Selectively Swollen Phases of Diblock Copolymers

D. Izzo[†] and C. M. Marques*,[‡]

Instituto de Física da Universidade Federal do Rio de Janeiro, Caixa Postal 68528, 21945-970 Rio de Janeiro, Brazil, and R.P.-C.N.R.S., Complex Fluids Laboratory UMR166, Cranbury, New Jersey 08512-7500

ABSTRACT: We study the aggregation of diblock copolymers in a selective solvent as a function of the asymmetry of the copolymer chains. When the shorter block is in a poor solvent, our mean-field approach predicts copolymer micellization in spherical or cylindrical geometries. For large collapsed blocks a dense lamellar phase is formed in an excess of solvent. A further increase of the size of the molten blocks leads to the formation of reverse micellar structures, where small spherical swollen cores are surrounded by a majority matrix of molten chains.

I. Introduction

Diblock copolymers self-assemble in a selective solvent,[1,2] a process that can be regarded as a macromolecular analog for micellization in solutions of low molecular weigth surfactants.[3] At very low concentrations isolated chains are dispersed in the solution. These chains have a tadpole configuration, with a collapsed head and a swollen tail. Above the critical micellar concentration the tadpole heads minimize the area exposed to the poor solvent by sharing the volume in the center of the micelle. This central core is surrounded by a shell of well-swollen chains. The geometry of the dilute micellar aggregates is determined by the copolymer asymmetry. For swollen tails much larger than the collapsed heads, the copolymers form spherical micelles. A reasonable agreement has been found between experiments[4] and existing theories[5−7] for spherical micellization, at least when thermodynamic equilibrium can be reached.[8] The existence of cylindrical aggregates is of a more controversial nature. They have been extensively studied for small molecular weight surfactants where they are also known as living polymers, wormlike micelles, giant micelles, or even as vermicelles.[9] They have been also reported in mixtures of diblock copolymers and homopolymers,[10] but to our knowledge no vermicelles have been observed in dilute solutions of diblock copolymers in a selective solvent. Mean-field theories predict that as the ratio betwen the collapsed block and tail lengths is increased, spherical micelles will no longer be stable and vermicelles will be formed. If this ratio is further increased, one expects that solubilization of the aggregates should no longer be possible, and the copolymers must phase separate into a dense organized phase coexisting with an excess of solvent. The reasons for phase separation are 2-fold. On one hand solubility is ensured by the presence of the swollen tail. If this block is too small, the isolated chains can no longer remain in solution. On the other hand a larger collapsed block also implies the onset of a lamellar phase at some chain asymmetry. Because copolymer bilayers have very large bending constants, the usual stabilization mechanism by Helfrich fluctuations[11] is inoperative for this system. Therefore, the condensed lamellar phase dissolves only the amount of solvent necessary to swell the tails and expels any

additional solvent. At the level of a scaling analysis both of these mechanisms predict a phase separation from a dilute to a condensed organized phase when $N_A \simeq N_B{}^{3/2}$, where N_A and N_B are respectively the polymerization indices of the collapsed and swollen blocks. The first condensed aggregate that appears upon increasing the collapsed block size is the lamellar phase, but other structures are expected to form by further increasing the collapsed block size. In this limit we consider reverse micellar structures consisting of small swollen cores embedded in a large matrix of molten polymers (see Figure 1).

A second pratical reason for studying the condensed phases is related to the preparation conditions of melts of diblock copolymers. These can be found in a variety of different crystalline structures, with periodicity values in the mesoscopic range of 5−500 nm. The different observed morphologies are determined by two parameters: the degree of incompatibility between different blocks and their relative molecular weight.[12] The degree of incompatibility is for melts measured by the product χN, where χ is the strength of the interactions between monomers of different blocks and N the total polymerization index of the chains. In practice, a strong segregation of the two blocks, leading to sharp interfaces between the different domains is achieved for χN values larger than 15. In order to achieve a high degree of segregation, one needs however to use rather large molecular weights. For instance, a typical value of χ of order of 0.1 would imply using chains with a molecular weigth of tens of kilograms per mole. However many chains with a high molecular weight are vitreous at room temperature. Therefore, exposing the macromolecules to a solvent is often a required intermediate state to prepare the liquid crystalline phases of diblock copolymers; this allows for a faster transition kinetics by the plasticizing effect of the solvent on the vitreous blocks.

In this paper we study the structure of the copolymer aggregates in an excess of selective solvent, for the full asymmetry range. As explained above direct micelles are expected for small sizes of the collapsed blocks. In the next section we review the theoretical predictions for these large asymmetry values. Section III studies the reversed copolymer phases within a mean-field theory. The last section summarizes our main results.

[†] Instituto de Física da Universidade Federal do Rio de Janeiro.
[‡] R.P.-C.N.R.S.

II. Direct Structures

We consider the formation of dilute cylindrical and spherical structures of AB diblock copolymer chains in
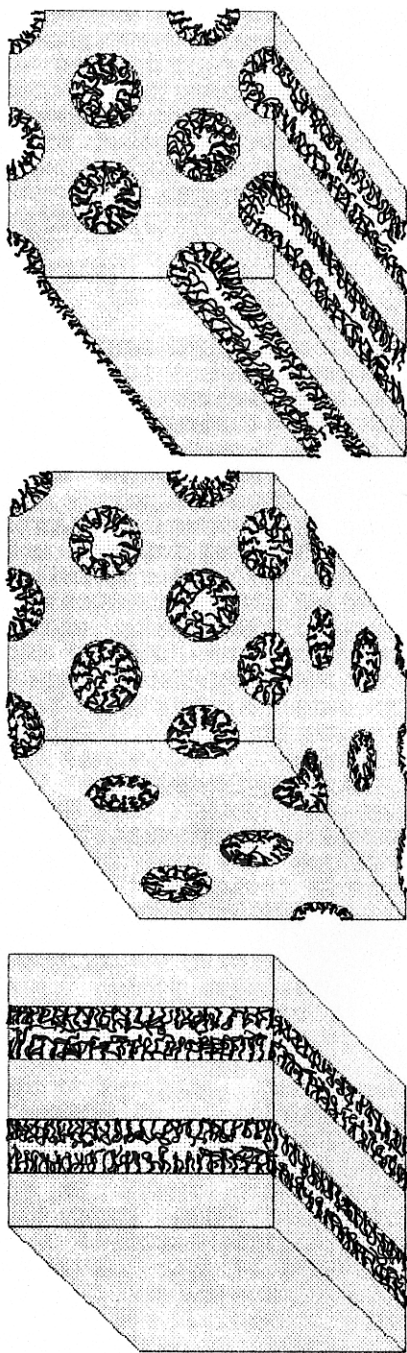
Figure 1. Reverse periodic strucutures which might occur in the limit of large molten blocks.

the presence of a solvent poor for block A and good for block B. We take the usual limit of maximum selectivity with no solvent penetration in the core and athermal solvent conditions in the corona. We will refer to these as the direct structures. We also determine the onset of phase separation into a dense phase by studying the transition into a lamellar geometry. As for copolymer melts, the structure of the aggregates is determined by two parameters: the strength of the interfacial energy γ between the collapsed monomers and the solvent, and the relative value of the polymerization indices of the two blocks N_A and N_B. Here however, the asymmetry is not given simply by the ratio $N_A/(N_A + N_B)$, but is a different function of these two numbers. In order to determine the asymmetry functions relevant for our study, we write the three main contributions to f, the free-energy per chain in a given geometry
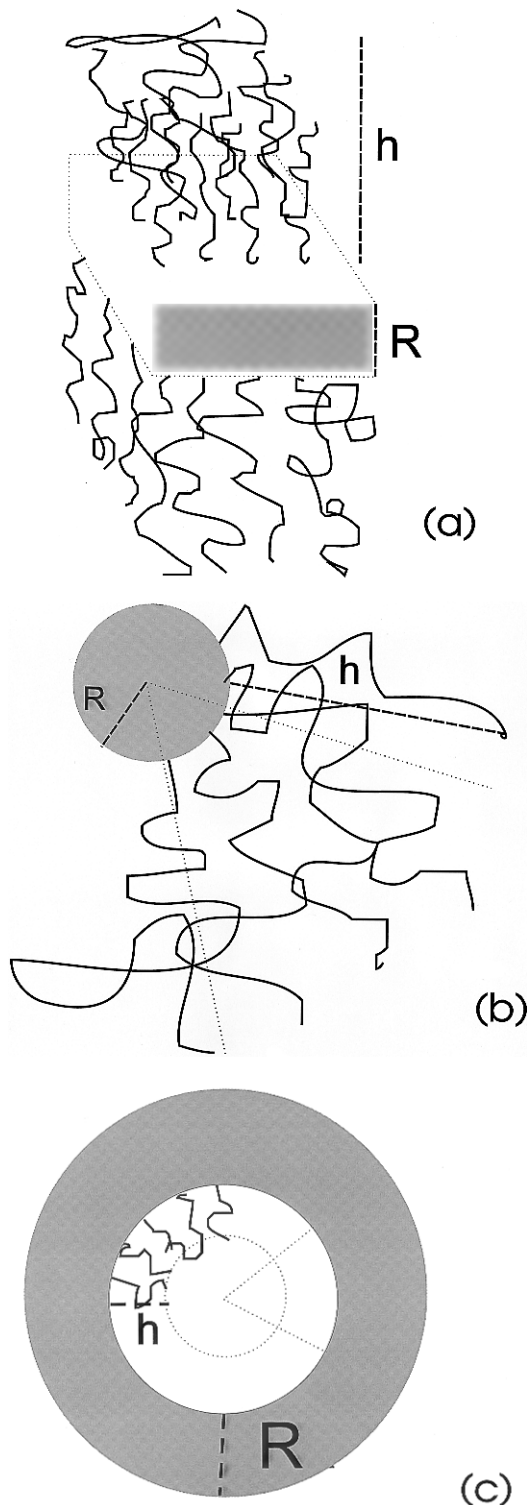

Figure 2. Wigner−Seitz cells corresponding to (a) lamellar strucuture, (b) direct curved structures, and (c) inverted curved structures. (b) and (c) represent either cylindrical or spherical configurations

$$f = f_\gamma + f_A + f_B \qquad (1)$$

where f_γ is the interfacial energy that accounts for the area exposed to the solvent, f_A is the stretching energy of a block in the molten region of the aggregate, and f_B the osmotic contribution of the swollen blocks. Let R be the size of the collapsed region, σ the number of copolymer junction points per unit surface, and h the size of the swollen regions (see Figure 2). For the direct structures the incompressibility of the core regions also

implies that $R = dN_A a\sigma$, where a is the monomer size, $d = 1$ for lamellas, $d = 2$ for cylinders, and $d = 3$ for spheres. We measure hereafter all lengths in units where $a = 1$. The size of the swollen chains being also a function of the chain density σ ($h \sim N_B \sigma^{1/3}$), we will choose for convenience h as the independent variable. The three contributions in eq 1 scale as (in energy units where $K_B T = 1$) $f_\gamma \sim \gamma/\sigma \sim \gamma N_B^3/h^3$, $f_A \sim R^2/N_A \sim h^6 N_A/N_B^6$ and $f_B \sim h^2/N_B$, where we have assumed mean-field expressions for the contributions of both the molten and the swollen chains. For large swollen blocks one expects the interfacial and corona contributions to dominate the free energy. The thickness of the swollen layer scales therefore as $h \sim N_B^{4/5}\gamma^{1/5}$, and the two other related quantities scale as $\sigma \sim (\gamma/N_B)^{3/5}$ and $R \sim N_A(\gamma/N_B)^{3/5}$. Exact coefficients can be determined from the expressions discussed below. An important point is that chains in the corona are very stretched, and chains in the core become stretched ($R \gg N_A^{1/2}$) for large enough collapsed blocks $N_A \gg N_A^s = N_B^{6/5}\gamma^{-6/5}$. However, it can be checked from eq 1 that the elastic energy of the A chains dominates only the free energy for large enough sizes of the collapsed blocks: $N_A \gg N_A^\beta = N_B^{9/5}\gamma^{-4/5}$. One expects the shape transitions to occur in the direct micelles when the sizes of both the collapsed and the swollen regions are of the same order, $h \simeq R$. This occurs when $N_A \simeq N_A^\alpha = N_B^{7/5}\gamma^{-2/5}$. We also anticipate that a last important point in the asymmetry range corresponds to the asymmetry value where curvature corrections to the osmotic energy become of the same order of the elastic energy of the molten chains. This can be checked to happen at $N_A = N_A^\epsilon = N_B^{8/5}\gamma^{-3/5}$.

To summarize these results we recapitulate the four mean-field asymmetry points in this problem: $N_A^s < N_A^\alpha < N_A^\epsilon < N_A^\beta$. As we increase the size of the collapsed blocks from a small value, the molten chains in the core start to stretch at $N_A = N_A^s$. At $N_A = N_A^\alpha$ the size of the swollen corona is of the same order as the size of the molten core. At $N_A = N_A^\epsilon$ the curvature corrections to the free energy are of the same order of the elastic energy in the core, we will see below that this is the point where the transitions to inverse structures occur. Finally at $N_A = N_A^\beta$ the elastic energy of the chains in the core dominates the free energy of the aggregates. It is also important to stress that our choice of mean-field expressions for the osmotic contribution is due to computational reasons. In fact, contrary to results from scaling, approximate analytic forms for these contributions are available for all the cases studied below, therefore allowing for a numerical study of the phase diagram. The main consequence of introducing the appropriate scaling exponents into the osmotic contribution of the corona is to change the functional form of the four asymmetry points discussed above, all the different regimes remaining unchanged. We quote here results from ref 13 that provides scaling results for these four points: $N_A^s = 1$, $N_A^\alpha = N_B^{15/11}\gamma^{-4/11}$, $N_A^\epsilon = N_B^{3/2}\gamma^{-3/2}$, $N_A^\beta = N_B^{18/11}\gamma^{-7/11}$.

Analytic expressions for the different stretching contributions to eq 1 have been calculated in the literature,[14-17] which we summarize in the Appendix; in the following we discuss the main approximations involved in those expressions. For the direct structures the chains in the cylindrical or the spherical cores can be viewed as polymer chains grafted to a concave dividing surface. In the limit of strong stretching, results of Semenov[14] and Witten, Milner, and Cates (S&W.M.C.)[15-17] provide an exact expression for the
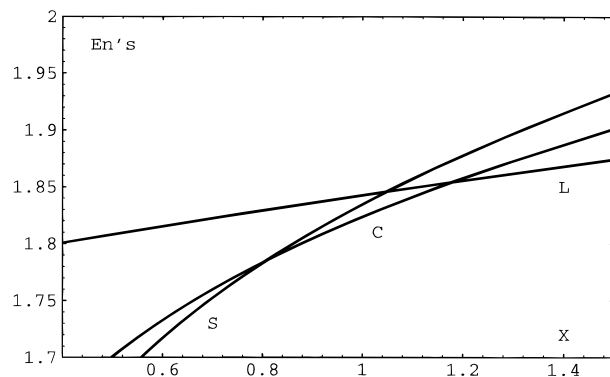

Figure 3. Energy of the direct structures as a function of $x \equiv N_A/N_A^\epsilon$: L, lamellae; C, cylinders; S, spheres.
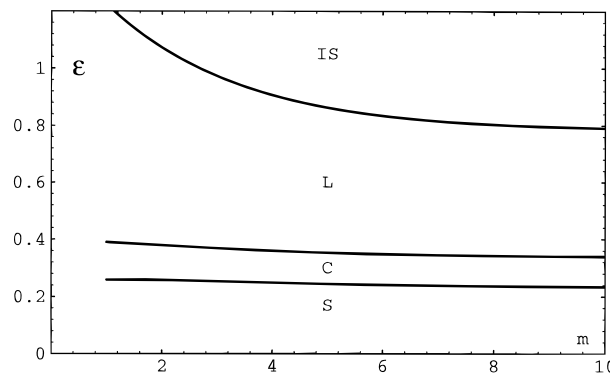

Figure 4. Phase diagram for diblock copolymers in a selective solvent. For this particular diagram the free-energy contributions of the molten chains in the inverse geometry have been calculated with the A-dG approximation. The X-axis is a logarithmic representation of the N_B values that are spanned by setting $N_B = 10^m$. The Y-axis represents the value of the asymmetry ratio N_A/N_A^ϵ. Key: L, lamellae; C, cylinders; S, spheres; IS, inverted spheres.

elastic and osmotic contribution of the chains free energy. The chains in the cylindrical or the spherical *coronas* can be regarded as being effectively grafted to a convex dividing surface. For this case the S&W.M.C. results only provide an approximate expression for the free energy contributions. However when comparing free energies, we expect the results to be reasonably accurate (this is known to hold for instance when computing the phase diagrams of copolymer melts). For the lamellar structure, S&W.M.C. expressions are exact for both the molten and the swollen layers.

In Figure 3 we compare the minimized values of the free energy of eq 1 as a function of the asymmetry ratio N_A/N_A^α, for the particular value of $N_B = 10^{5/2} \simeq 316$ (for simplicity we set hereafter $\gamma = 1$). Each one of the three phases considered has a region of stability in this phase diagram. The cylindrical phase is stable close to the point $N_A = N_A^\alpha$. As expected, large swollen blocks ($N_A \ll N_A^\alpha$) lead to the formation of spherical micelles, whereas large collapsed blocks ($N_A \gg N_A^\alpha$) have a tendency to form lamellar phases. In Figure 4 the asymmetry points for the spherical-cylindrical and cylindrical-lamellar transitions is plotted in the phase diagram [$N_A/N_B^{8/5}$, m]. The X-axis is a logaritmic representation of the N_B values that are spanned by setting $N_B = 10^m$. The Y-axis represents the value of the asymmetry ratio N_A/N_A^ϵ at which the different transitions occur. For all explored asymmetries the spherical micelles are the stable aggregates for small collapsed blocks, and cylindrical and lamellar aggregates appear upon an increase of the collapsed block
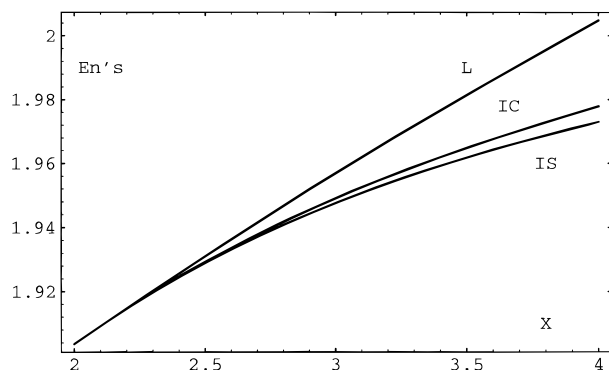
Figure 5. Energy of the inverted structures as a function of $x \equiv N_A/N_A{}^\epsilon$, within the S&W.M.C. approximation for the molten chains: L, lamellae; IC, inverted cylinders; IS, inverted spheres. The inverted spheres are always the stable structure.

Figure 6. Phase diagram for diblock copolymers in a selective solvent. For this particular diagram the free-energy contributions of the molten chains in the inverse geometry have been calculated with the S&W.M.C. approximation. The *X*-axis is a logarithmic representation of the N_B values that are spanned by setting $N_B = 10^m$. The *Y*-axis represents the value of the asymmetry ratio $N_A/N_A{}^\epsilon$. Key: C, cylinders; S, spheres; IS, inverted spheres.

sizes. We now investigate the geometry of the aggregates formed under a further increase of the collapsed block size.

III. Reverse Structures

We consider the formation of reverse cylindrical and spherical structures of AB diblock copolymer chains exposed to a selective solvent, poor for block A. In the limit where A blocks are very large, the structures that we consider can be regarded as swollen holes organized in a majority matrix of molten blocks (see Figures 1 and 2c). We assume that the copolymer sample is exposed to an excess of selective solvent such that the equilibrium state of swelling of the B blocks can be attained. In contrast to the previous section where we explored N_A values smaller than or of the order of $N_A{}^\alpha = N_B{}^{7/5}$, we scan here the range $N_A \gg N_B{}^{7/5}$.

Technically, the minimization of eq 1 with expressions for the free energies of the inverted structures is more involved than the corresponding minimization for the direct structures. The increased difficulty stems from the fact that now the radius R of the surface separating the molten and the swollen regions is a second independent variable that will adjust to equilibrium conditions. In fact the equilibrium R value will determine how much solvent the structure can accommodate. The height of the swollen chain can still be regarded as a function of the grafting density σ; we thus choose to minimize eq 1 with respect to the two variables h and R. A comparison of the stretching energies and interfacial tension shows that the scaling form for the radius is $R \sim N_B$, the exact numerical coefficient being always of order unity. The sizes of the swollen holes are larger than the height of the corona therein, by a factor $N_B{}^{1/5}$. Also the solvent fraction present in the sample is $\phi = R^3/R_T{}^3$ with $R_T{}^3 \sim (N_A\sigma R^2)^3$ the volume occupied by the chains grafted to the surface of one hole. From the above results, $\sigma \sim N_B{}^{-3/5}$ and one gets a volume fraction $\phi \sim N_B{}^{8/5}/N_A = (N_A/N_A{}^\epsilon)^{-1}$, which is of order 1 at the transition asymmetry $N_A{}^\epsilon$. Diblock copolymers in this composition range should be able to host a finite fraction of selective solvent.

The geometry of the solvent holes is determined by minimization of (1) with the appropriate energy expressions given in the Appendix. We present in Figure 5 results for the minimized free energies of a diblock copolymer system similar to the one studied in the previous section: $N_B = 10^{5/2}$ and $N_A \gg N_A{}^\alpha$. In this figure both swollen and molten chains are described by free energies of the S&W.M.C. approximation. This
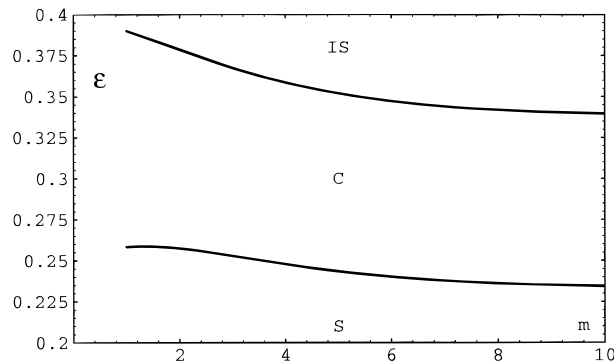
formalism is known to describe exactly the swollen chains grafted to a concave surface but to underestimate the energy of the molten chains which are grafted to a convex surface. As the figure shows, for $N_B = 10^{5/2}$, the spherical inverted structures are the only stable inverted geometry, even if for a relatively large range of N_A values the three studied structures have very similar energies. More generally, Figure 6 displays the transition points from the direct spheres to direct cylinders and from the direct cylinders to inverted spheres for a large range of N_B values. In the studied range, inverted micelles are the only stable structure.

In order to raise the degeneracy in the S&W.M.C. expressions for the inverted structures, we also minimized the total free energy using the Alexander–de Gennes (A–dG) approximation[18,19] for the molten chains. The justification for this procedure is the following. The S&W.M.C. picture of a grafted layer assumes that the chain ends are distributed over the height of the layer. However, for convex surfaces, the chain ends are known to avoid a region close to the surface, known as the exclusion zone. This increases the elastic energy of the system. If the exclusion zone had the size of the layer, then all the ends would be confined at the outer surface of the grafted layer. This is the explicit assumption in the A–dG model of the grafted layers. The free energy of a polymer layer grafted to a convex surface is therefore intermediate between the S&W.M.C. and the A–dG values. Using the expressions derived by these last authors allows for an estimation of an upper bound for the free energy. More accurate predictions for the actual free energy, in the range of parameters relevant to the phase diagram, might soon become available by further extensions of the variational approach developed in ref 20 or perhaps by extending the work of Olmestd and Milner.[21,22] Also self-consistent numerical calculations might also allow refinement of the picture presented here.

Figures 4 and 7 present the modifications introduced to the phase diagrams by the A–dG expressions. The energy values of the lamellae, inverted cylinders, and inverted micelles are well resolved. A finite window in the asymmetry diagram is now open for the lamellar phase. However the inverted cylinders are never present in the diagram.
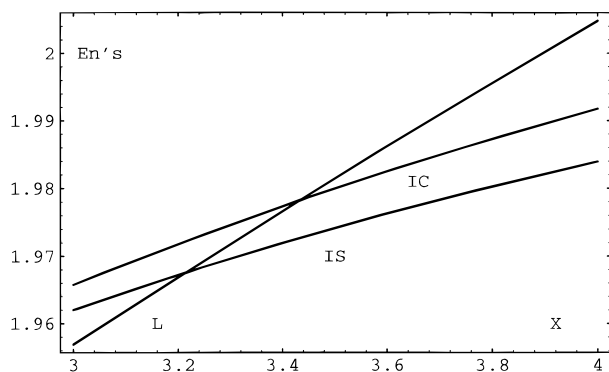
Figure 7. Energy of the inverted structures as a function of $x \equiv N_A/N_A^\epsilon$, calculated within the A−dG approximation for the molten chains: L, lamellae; IC, inverted cylinders; IS, inverted spheres. The inverted cylindrical structures are never present on the diagram.

IV. Conclusions

In this paper we studied the formation of micelle aggregates of diblock copolymers in a selective solvent. Using a mean-field analysis we predict the formation of direct spherical and cylindrical micelles and of lamellar and inverted spherical phases upon increasing sizes of the blocks in a poor solvent. No inverted cylindrical phase is predicted to be stable. These shape transitions for direct structures occur for asymmetry parameters $N_A/N_B^{7/5}$ of order unity. Transition into reverse shapes is controlled by the asymmetry function $N_A/N_B^{8/5}$.

We have restricted our analysis to the three simplest possible phases, which are representative of one-, two-, and three-dimensional geometries. At this level the approximation of a circular Wigner-Seitz cell is sufficient to resolve aggregates in the three geometries but precludes the distinction between different phases with the same dimensionality. It would also be important, as an extension of this work, to further investigate the presence of bicontinuous phases. However, a first indication that reverse structures of these phases migth have a poor stability is provided by the absence of the reverse cylindrical phase, and therefore by the absence of a cylindrical−lamellar border where the bicontinuous phases are located.

Birshtein and Zhulina[23] have addressed a similar problem by forcing each of the blocks N_A and N_B to be solvated at concentrations c_A and c_B. In contrast, we studied the case where the solvent is selective ($c_A = 1$) and the system self-adjusts to the appropriate c_B values when exposed to a solvent reservoir. Moreover, here we restrict ourselves to a mean-field analysis, for which the numerical factors are known.

In a previous paper we studied the direct micellar structures by using an asymptotic analysis of scaling forms for the different free energy contributions. We did not find any asymptotically large window for stable cylindrical geometries, a result in agreement with the present mean-field result which confines the window range of cylindrical stability to a small region around $N_A \simeq N_B^{7/5}$. In the appropriate scaling framework this asymmetry has a different power law dependence and would correspond to $N_A \simeq N_B^{15/11}$.

An interesting feature of the inverted spherical structures is that the size of the solvent hole is always larger than the height of the corona hosted therein. The volume fraction ϕ of the solvent that the sample can accommodate decreases with increasing asymmetry, $\phi \sim N_B^{8/5}/N_A$.

Further developments of this work should consider the question of the solvent molecular weight. Indeed, in the context of copolymer/homopolymer blends it is known[10] that cylindrical structures exist when the homopolymer is the majority component (direct vermicelles), it would be important to know if they persist in the reverse situation where the homopolymer is the minority component. Interestingly, this is also related to the question of the embedding of solid particles in diblock copolymer phases,[24] in both situations the corona being a molten polymer layer.

Appendix

Here we present general expressions for the free-energy contribution to eq 1 for the different geometries. The total free energy is then minimized to determine the stability of the structures as a function of the polymerization indices N_A and N_B. All expressions are written in energy units where $k_B T = 1$ and length units where $a = 1$.

The interfacial contribution f_γ per chain is

$$f_\gamma = \gamma/\sigma \qquad (2)$$

For the lamellar geometry, the S&W.M.C. contributions for the molten A and swollen B blocks (see Figure 2a) are

$$f_A = \frac{\pi^2}{24} N_A \sigma^2 \qquad (3)$$

and

$$f_B = \frac{3\pi^2}{40} \frac{h^2}{N_B} \qquad (4)$$

The height of the swollen brush h and the chain density σ are related by $\sigma = (\pi^2/12N_B^3)h^3$. As explained in section II, the natural rescaling variables for the different quantities are $\tilde{h} = hN_B^{-4/5}\gamma^{-1/5}$, $\tilde{\sigma} = \sigma N_B^{3/5}\gamma^{-3/5}$, and $\tilde{f} = fN_B^{-3/5}\gamma^{-2/5}$. Expressions 2, 3, and 4 and can be rewritten as

$$\tilde{f}_\gamma = 1/\tilde{\sigma} \qquad (5)$$

$$\tilde{f}_A = \frac{\pi^2}{24} \beta \tilde{\sigma}^2 \qquad (6)$$

and

$$\tilde{f}_B = \frac{3\pi^2}{40} \tilde{h}^2 \qquad (7)$$

with $\tilde{\sigma} = (\pi^2/12)\tilde{h}^3$ and $\beta = N_A/N_B^{9/5}$. Hereafter, we will be using renormalized quantities as defined above.

For the direct cylindrical geometry (see Figure 2b)

$$\tilde{f}_\gamma = 1/\tilde{\sigma} \qquad (8)$$

$$\tilde{f}_A = \frac{\pi^2}{12} \beta \tilde{\sigma}^2 \qquad (9)$$

and

$$\tilde{f}_B = \frac{3\pi^2}{40} \, \tilde{h}^2 \, \frac{1 + \frac{5}{12}\epsilon\frac{\tilde{h}}{\tilde{R}}}{1 + \frac{3}{8}\epsilon\frac{\tilde{h}}{\tilde{R}}} \tag{10}$$

with $\tilde{\sigma} = (\pi^2/12)\tilde{h}^3\,(1 + (3/8)\epsilon(\tilde{h}/\tilde{R}))$. For the direct structures, the radius of the cylinder $R = 2N_A\sigma$ has been renormalized according to $\tilde{R} = RN_B^{3/5}N_A^{-1}\gamma^{-3/5}$.

For the inverted cylindrical geometry (see Figure 2c)

$$\tilde{f}_\gamma = 1/\tilde{\sigma} \tag{11}$$

where

$$\tilde{f}_A = \frac{\pi^2}{48}\,\epsilon\tilde{R}^2\Big[12 + 3u + \frac{8}{u}(1 - (1 + u)^{3/2})\Big],$$
$$\text{for S\&W.M.C.} \tag{12}$$

$$\tilde{f}_A = \frac{1}{4}\sqrt{\beta\epsilon}\frac{\tilde{\sigma}}{\tilde{R}}\ln(1 + u), \quad \text{for A$-$dG} \tag{13}$$

$$u = 2\,\sqrt{\frac{\beta}{\epsilon}}\frac{\tilde{\sigma}}{\tilde{R}}$$

and

$$\tilde{f}_B = \frac{3\pi^2}{40}\,\tilde{h}^2\,\frac{1 - \frac{5}{12}\sqrt{\beta\epsilon}\frac{\tilde{h}}{\tilde{R}}}{1 - \frac{3}{8}\sqrt{\beta\epsilon}\frac{\tilde{h}}{\tilde{R}}} \tag{14}$$

with $\tilde{\sigma} = (\pi^2/12)\tilde{h}^3\,(1 - (3/8)\sqrt{\beta\epsilon}(\tilde{h}/\tilde{R}))$. For the inverted structures the radius R of the cylindrical holes is an independent variable with a different renormalization, $\tilde{R} = RN_B^{-1}$.

The spherical counterparts of the above expressions are the following. For the direct spheres (see Figure 2b)

$$\tilde{f}_\gamma = 1/\tilde{\sigma} \tag{15}$$

$$\tilde{f}_m = \frac{3\pi^2}{80}\beta\tilde{\sigma}^2 \tag{16}$$

and

$$\tilde{f}_b = \frac{3\pi^2}{40}\,\tilde{h}^2\,\frac{1 + \frac{5}{6}\epsilon\frac{\tilde{h}}{\tilde{R}} + \frac{5}{21}\epsilon^2\big(\frac{\tilde{h}}{\tilde{R}}\big)^2}{1 + \frac{3}{4}\epsilon\frac{\tilde{h}}{\tilde{R}} + \frac{1}{5}\epsilon^2\big(\frac{\tilde{h}}{\tilde{R}}\big)^2} \tag{17}$$

with $\tilde{\sigma} = (\pi^2/12)\tilde{h}^3\,(1 + (3/4)\epsilon(\tilde{h}/\tilde{R}) + (1/5)\epsilon^2(\tilde{h}/\tilde{R})^2)$. For the direct structures, the radius of the sphere $R = 3N_A\sigma$ has been renormalized according to $\tilde{R} = RN_B^{3/5}N_A^{-1}\gamma^{-3/5}$.

For the inverted spheres (see Figure 2c)

$$\tilde{f}_\gamma = 1/\tilde{\sigma} \tag{18}$$

$$\tilde{f}_m = \frac{\pi^2}{80}\,\epsilon\tilde{R}^2\Big[10 + 9v - \frac{15}{v}(1 + v)^{4/3} + \frac{6}{v}(1 + v)^{5/3}\Big],$$
$$\text{for S\&W.M.C.} \tag{19}$$

$$\tilde{f}_A = \frac{1}{2}\sqrt{\beta\epsilon}\,\frac{\tilde{\sigma}}{\tilde{R}}\Big[1 - \frac{1}{(1 + v)^{1/3}}\Big], \quad \text{for A$-$dG} \tag{20}$$

where

$$v = 3\sqrt{\frac{\beta}{\epsilon}}\frac{\tilde{\sigma}}{\tilde{R}}$$

and

$$\tilde{f}_B = \frac{3\pi^2}{40}\,\tilde{h}^2\,\frac{1 - \frac{5}{6}\sqrt{\beta\epsilon}\frac{\tilde{h}}{\tilde{R}} + \frac{5}{21}\beta\epsilon\big(\frac{\tilde{h}}{\tilde{R}}\big)^2}{1 - \frac{3}{8}\sqrt{\beta\epsilon}\frac{\tilde{h}}{\tilde{R}} + \frac{3}{4}\beta\epsilon\big(\frac{\tilde{h}}{\tilde{R}}\big)^2} \tag{21}$$

with $\tilde{\sigma} = (\pi^2/12)\tilde{h}^3\,(1 - (3/4)\sqrt{\beta\epsilon}(\tilde{h}/\tilde{R}) + (1/5)\beta\epsilon(\tilde{h}/\tilde{R})^2)$. For the inverted structures the radius R of the spherical holes is an independent variable with a different renormalization, $\tilde{R} = RN_B^{-1}$.

References and Notes

(1) Gallot, Y.; Franta, E.; Rempp, P.; Benoit, H. *J. Polym. Sci.* **1964**, *4*, 473.
(2) Tuzar, Z.; Kratochvil, P. *Adv. Colloid Interface Sci.* **1976**, *6*, 201.
(3) Napper, D. H. *Polymeric Stabilization of Colloidal Dispersions*; Academic Press: London, 1983.
(4) Xu, R. L.; Winnik, M. A.; Riess, G.; Chu, B. *Macromolecules* **1992**, *25*, 644.
(5) Halperin, A. *Macromolecules* **1987**, *20*, 2943.
(6) Marques, C. M.; Joanny, J. F.; Leibler, L. *Macromolecules* **1988**, *21*, 1051.
(7) Vagberg, L. J. M.; Cogan, K. A.; Gast, A. P. *Macromolecules* **1991**, *24*, 1670.
(8) Marques, C. M. *Langmuir* **1997**, *13*, 1430.
(9) Cates, M. E.; Candau, S. J. *J. Phys.: Cond. Matter.* **1990**, *2*, 6869.
(10) Kinning, D. J.; Winey, K. I.; Thomas, E. L. *Macromolecules* **1988**, *21*, 3502.
(11) Safran, S. A. *Statistical Thermodynamics of Surfaces, Interfaces and Membranes*; Addison-Wesley: Reading, MA, 1994.
(12) Leibler, L. *Macromolecules* **1980**, *13*, 1602.
(13) Izzo, D.; Marques, C. M. *Macromolecules* **1993**, *26*, 7189.
(14) Semenov, A. N. *Sov. Phys. JETP* **1985**, *61*, 733.
(15) Milner, S.; Witten, T.; Cates, M. *Europhys. Lett.* **1988**, *5*, 413.
(16) Milner, S.; Witten, T.; Cates, M. *Macromolecules* **1989**, *22*, 853.
(17) Milner, S.; Witten, T. *Macromolecules* **1988**, *49*, 1951.
(18) Alexander, S. *J. Phys. (Paris)* **1977**, *38*, 983.
(19) de Gennes, P. G. *J. Phys. (Paris)* **1976**, *37*, 1443.
(20) Li, H.; Witten, T. A. *Macromolecules* **1994**, *27*, 449.
(21) Olmsted, P.; Milner, S. T. *J. Phys. II (Paris)* **1997**, *7*, 249.
(22) Olmsted, P.; Milner, S. T. *Phys. Rev. Lett.* **1994**, *72*, 936.
(23) Birshtein, T. M.; Zhulina, E. B. *Polymer* **1990**, *31*, 1312.
(24) Turner, M. S.; Marques, C. M. *Europhys. Lett.* **1995**, *32*, 493.

MA970264E